

# A New Technique for Measuring the Constitutive Parameters of Planar Materials

Waymond R. Scott, Jr., *Member, IEEE*

**Abstract**—A technique for measuring the constitutive parameters of materials over a broad range of frequencies is developed in this work. The technique is specifically designed for planar samples. Planar samples can be placed in the measurement fixture without any special preparation; this makes the technique more convenient than other techniques which require that the sample be machined to fit into a measurement fixture. The finite element method is used in the analysis of the fixture. Using fourth-order elements, the finite element method provides a general, very accurate solution. The technique is experimentally verified by measuring the constitutive parameters of two materials with known properties. The measured results are compared to those of other investigators and are shown to be in good agreement.

## I. INTRODUCTION

A technique which is specifically designed for measuring the constitutive parameters of planar samples over a broad range of frequencies is investigated in this work. Fig. 1 is a sketch of the fixture that is used in the technique. The material to be measured is placed between the two conducting plates which are attached to the coaxial lines. A planar sample can be placed in the fixture without any preparation; this is a definite advantage over techniques which require the sample to be precisely machined to fit into a waveguide, coaxial line, or other measurement fixture. In many of these techniques, the preparation of the sample is the most difficult part of the measurement procedure.

In the technique, the reflection coefficient and/or the transmission coefficient of the fixture are/is measured. If both are measured, both the complex permittivity and the complex permeability can be determined. If only one is measured, either the complex permittivity or the complex permeability can be determined. This step requires a very accurate relationship between the constitutive parameters and the reflection and transmission coefficients. Such a relationship cannot be determined analytically and must be determined numerically. The finite element method (FEM) is used to determine the relationship in this work. Fourth-order elements are used in the FEM in order to

Manuscript received October 31, 1991; revised April 24, 1992. This work was supported in part by the Georgia Tech Material Metrology Consortium, the Georgia Tech Manufacturing Research Center, and the Joint Services electronics Program under Contracts DAAL-03-87-K-0059 and DAAL-03-90-C-0004.

The author is with the School of Electrical Engineering, Georgia Institute of Technology, Atlanta, GA 30332-0250.

IEEE Log Number 9202491.

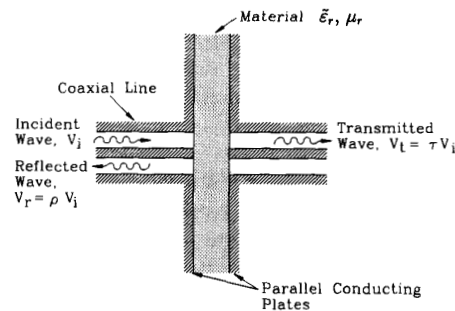


Fig. 1. Cross section of the measurement fixture.

obtain sufficient accuracy with reasonable computational efficiency. The technique is verified experimentally by measuring the constitutive parameters of materials with known properties.

## II. MEASUREMENT FIXTURE

The measurement fixture can be used in two configurations: in the first, the radial transmission line formed by the conducting plates is terminated with a metallic wall, and in the second, the radial transmission line is left open. The first configuration is easier to model accurately since it has a closed boundary except for the input and output ports; the metallic wall terminating the radial line can be modeled as a perfect electric conductor. However, with this configuration, the sample must be machined into a cylindrical shape before it can be placed in the fixture. The second configuration is more difficult to model since the radial transmission line is left open. However, with this configuration, a planar sample can be placed in the fixture without modification. In this work, the second configuration will be used, and the open end will be modeled by a perfectly conducting magnetic wall. Even though this model is only approximate, it will be shown that it is sufficiently accurate for a certain range of frequencies. The model is easily incorporated into the finite element method, and the model is relatively good when the spacing between the plates is much less than a half of a wavelength in the sample. A better model would require that the geometry for the sample beyond the open end of the radial transmission be known. This would make the technique less useful, because it would require the sample to be machined into a certain shape, or it would require the geometry of the sample to be entered into the model.

This work will concentrate on the second configuration since it does not require any machining of a planar sample. However, the finite element analysis developed in this work will accurately model the fixture in both configurations. Recently, Saed has investigated a similar fixture which is operated in the first configuration, and he analyzed it using a method of moments [1]. Others have investigated a related technique which also requires the sample to be machined into a cylindrical shape [2]–[3]. In this technique, the outer conductor is continuous, and the sample is placed in a gap between the center conductors. These investigators used a mode-matching technique in the analysis of their measurement fixture.

In order to calculate the practical frequency range of the technique, a simple model is developed and investigated. Fig. 2 is a sketch of a simple model for the measurement fixture. The model consists of input and output transmission lines, a capacitor, and an open-circuited radial transmission line. The capacitor models the capacitive coupling between the center conductors, and the radial transmission line models the conducting plates in the fixture.

When the sample is placed in the measurement fixture, it fills most of the capacitor and all of the radial transmission line. The admittance of the capacitor is approximately

$$Y_c = j\omega C_c \approx j\omega \bar{\epsilon}_r C_{co} \quad (1)$$

where  $\bar{\epsilon}_r = \bar{\epsilon}/\epsilon_o = (\epsilon - j\sigma/\omega)/\epsilon_o$  is the complex relative permittivity of the sample, and  $C_{co}$  is the capacitance between the center conductors when the fixture is filled with free space. Here  $C_c$  is approximately  $\bar{\epsilon}_r C_{co}$  because the sample does not fill the entire capacitor; a portion of the fringing fields is not in the sample. The input admittance of the radial transmission line is

$$Y_r = \frac{2\pi b}{t} \frac{kb}{\eta \zeta(kb, c/b)} \quad (2)$$

where  $\zeta(kb, c/b) = (E_z/H_o)/(\eta/kb)$  is the normalized impedance at the input of the radial transmission line for a TEM wave [4],  $k = \omega\sqrt{\mu\bar{\epsilon}}$  is the wavenumber,  $\eta = \sqrt{\mu/\bar{\epsilon}}$  is the wave impedance,  $\mu_r = \mu/\mu_o$  is the complex relative permeability of the sample,  $b$  is the radius of the outer conductor of the coaxial line, and  $c$  is the outer radius of the radial line.

The reflection coefficient  $\rho$  and the transmission coefficient  $\tau$  of the fixture are primarily determined from the capacitance between the center conductors whenever the inequality

$$\left| \frac{Y_r}{Y_c} \right| \gg 1 \quad (3)$$

is satisfied. When the ratio  $|Y_r/Y_c|$  is large,  $\rho$  and  $\tau$  are less sensitive to  $Y_r$  than to  $Y_c$ ; then, the errors in  $\rho$  and  $\tau$  due to the approximation in modeling the open radial line

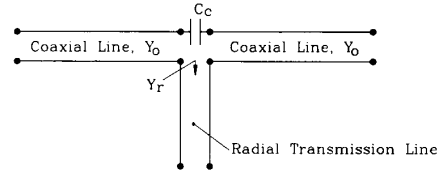


Fig. 2. Simple model for the measurement fixture.

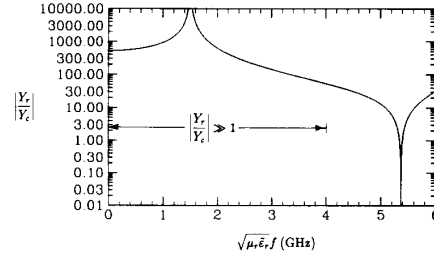


Fig. 3. Graph of the ratio  $|Y_r/Y_c|$  as a function of the normalized frequency with  $2b = 7$  mm and  $c/b = 10$ .

are very small. In this work, the frequency range will be restricted such that the ratio  $|Y_r/Y_c|$  is large. The ratio  $|Y_r/Y_c|$  is graphed as a function of normalized frequency in Fig. 3. In the calculations,  $2b = 7$  mm,  $c/b = 10$ , and the capacitance is approximated using the formula for an ideal parallel-plate capacitor:  $C_{co} \approx \epsilon_o \pi a^2/t$ ; then  $|Y_r/Y_c| \approx |2b^2/\zeta a^2|$  where  $a$  is the radius of the inner conductor of the coaxial line. The graph of the ratio is seen to have two cusps. At approximately 1.5 GHz the ratio is infinite because  $Y_r$  is infinite, and at approximately 5.2 GHz the ratio is zero because  $Y_r = 0$ ; the radial line is resonant at these frequencies. For the parameters chosen, the ratio is seen to be large for the frequency range  $0 \leq \sqrt{\mu_r \bar{\epsilon}_r} f \leq 4$  GHz. These parameters were chosen to yield a high ratio  $|Y_r/Y_c|$  for a large frequency range. The frequency of the second resonance is approximately inversely proportional to  $c$  when  $c/b \gg 1$ . At low frequencies, the ratio  $|Y_r/Y_c|$  is approximately equal to the ratio of the cross-sectional area of one of the conducting plates to that of the center conductor:  $|Y_r/Y_c| \approx (c^2 - b^2)/a^2$ . Decreasing  $c$  will increase the frequency of the second resonance; however, it will decrease the ratio  $|Y_r/Y_c|$ . Thus, decreasing  $c$  will only increase the frequency range if the minimum value of the ratio  $|Y_r/Y_c|$  is allowed to be smaller.

From this simple model, it is apparent that the technique is much more sensitive to the permittivity of the sample than to the permeability of the sample. This is because  $\rho$  and  $\tau$  are primarily determined by  $Y_c$  which is very insensitive to the permeability for the above frequency range. It is also apparent that  $\tau$  is more sensitive to the permittivity than  $\rho$ , especially at the lower frequencies where  $\tau \approx 2Y_c/Y_o \approx j2\omega \bar{\epsilon}_r C_{co}/Y_o$  and  $\rho \approx 1$ . Thus, for the experimental part of this work, only nonmagnetic samples are measured, and the permittivities of the samples are determined from  $\tau$ .

## III. FINITE ELEMENT ANALYSIS

The fields in the fixture are governed by Maxwell's two curl equations,

$$\nabla \times \vec{E} = -j\omega\mu\vec{H} \quad (4)$$

$$\nabla \times \vec{H} = j\omega\vec{\epsilon}\vec{E} \quad (5)$$

where an  $e^{j\omega t}$  time dependence is assumed. The vector Helmholtz equations are obtained from the curl equations,

$$\nabla \times \left( \frac{1}{\vec{\epsilon}} \nabla \times \vec{H} \right) = \omega^2 \mu \vec{H} \quad (6)$$

$$\nabla \times \left( \frac{1}{\mu} \nabla \times \vec{E} \right) = \omega^2 \vec{\epsilon} \vec{E}. \quad (7)$$

Only axisymmetric TM modes will exist in the fixture, because the fixture is axisymmetric and the incident wave is TEM:

$$\vec{H} = H_\phi(r, z)\hat{\phi} \quad (8)$$

$$\vec{E} = E_r(r, z)\hat{r} + E_z(r, z)\hat{z}. \quad (9)$$

Since only one component of  $\vec{H}$  exists, the vector Helmholtz equation for  $\vec{H}$  can be reduced to a single scalar equation in  $H_\phi$ :

$$\begin{aligned} \nabla \cdot \left( \frac{1}{\vec{\epsilon}_r} \nabla H_\phi \right) - \frac{1}{\vec{\epsilon}_r r^2} H_\phi + \mu_r k_o^2 H_\phi \\ + \frac{1}{r} \frac{\partial}{\partial r} \left( \frac{1}{\vec{\epsilon}_r} \right) H_\phi = 0 \end{aligned} \quad (10)$$

where  $k_o = \omega\sqrt{\mu_o\epsilon_o}$ . The two components of  $\vec{E}$  can be obtained from  $H_\phi$  using one of Maxwell's curl equations (5). A solution to (10) subject to the appropriate boundary conditions is determined using the FEM. Galerkin's method is used in the formulation [5], [6].

The region of interest is divided up into elements as in Fig. 4. The elements are arranged so that they are small where the field varies the quickest and are large where the field varies more slowly. The electric field in the fixture is singular at the corners of the inner and outer conductors ( $\nabla \cdot (rH_\phi)$  is singular); hence, the elements are smaller at the corners.

Even though the incident wave is a TEM mode, the discontinuity in the coaxial line will generate higher order modes; however, the frequency is restricted so that the higher order modes are cut off in the coaxial lines, and the distance that the finite element mesh extends into the coaxial lines is chosen to be sufficiently long so that the fields at the input and output planes of the mesh (ports) are essentially TEM. It was determined empirically that extending the mesh a distance of  $2b$  into the line is sufficient for this application.

The elements are generated by rotating the planar triangular elements about the  $z$ -axis to sweep out an annular volume. Let  $V^{(e)}$  be the volume swept out by element ( $e$ ),  $S^{(e)}$  be the surface of the volume,  $A^{(e)}$  be the cross-sectional

area of the planar element, and  $\Gamma^{(e)}$  be the boundary of the planar element. In Galerkin's method residual integrals are computed for each of the weighting functions  $W_i$ . The contribution of element ( $e$ ) to the residual integral for the weighting function  $W_i$  is

$$\begin{aligned} R_i^{(e)} = - \int_{V^{(e)}} W_i \left[ \nabla \cdot \left( \frac{1}{\vec{\epsilon}_r} \nabla H_\phi \right) - \frac{1}{\vec{\epsilon}_r r^2} H_\phi \right. \\ \left. + \mu_r k_o^2 H_\phi + \frac{1}{r} \frac{\partial}{\partial r} \left( \frac{1}{\vec{\epsilon}_r} \right) H_\phi \right] dV. \end{aligned} \quad (11)$$

This equation is rearranged to obtain a boundary integral in a form that allows the boundary conditions to be enforced in a straightforward manner:

$$\begin{aligned} R_i^{(e)} = - \oint_{S^{(e)}} W_i \frac{1}{\vec{\epsilon}_r} \nabla(rH_\phi) \cdot d\vec{S} \\ + \int_{V^{(e)}} \left\{ \frac{1}{\vec{\epsilon}_r} \nabla W_i \cdot \nabla H_\phi + \frac{1}{\vec{\epsilon}_r r} \hat{r} \cdot \nabla (W_i H_\phi) \right. \\ \left. + W_i \left[ \frac{1}{\vec{\epsilon}_r r^2} H_\phi - \mu_r k_o^2 H_\phi \right] \right\} dV. \end{aligned} \quad (12)$$

The weighting functions are chosen to be

$$W_i = \sqrt{r} \alpha_i(r, z) \quad (13)$$

and  $H_\phi$  is expanded in terms of the basis functions

$$H_\phi = \sum_j H_j \sqrt{r} \alpha_j(r, z) \quad (14)$$

where the  $\alpha$ 's are the usual finite element basis functions. The  $\sqrt{r}$  term is included to eliminate the  $1/r$  terms in (12); this makes it possible to evaluate and store the resulting integrals in universal matrices. The basis functions are the interpolation polynomials for the elements. Triangular elements of first order have three linear basis functions, and the triangular elements of order  $n$  have  $(n+1)(n+2)/2$  polynomial basis functions of order  $n$ , one for each node of the elements [7].

After using (13) and (14) and evaluating the  $\phi$  integral, (12) becomes

$$\begin{aligned} R_i^{(e)} = -2\pi \oint_{\Gamma^{(e)}} W_i \frac{1}{\vec{\epsilon}_r} \nabla(rH_\phi) \cdot d\vec{\Gamma} \\ + 2\pi \sum_j H_j \int_{A^{(e)}} \left\{ \frac{r^2}{\vec{\epsilon}_r} \nabla \alpha_i \cdot \nabla \alpha_j + \frac{3r}{2\vec{\epsilon}_r} \hat{r} \cdot \nabla(\alpha_i \alpha_j) \right. \\ \left. + \left[ \frac{9}{4\vec{\epsilon}_r} - \mu_r k_o^2 r^2 \right] \alpha_i \alpha_j \right\} dA \end{aligned} \quad (15)$$

where  $d\vec{\Gamma} = \vec{n} d\Gamma$  is normal to the boundary. Here  $\vec{\epsilon}_r$  and  $\mu_r$  are restricted to be constant in each element to simplify the evaluation of the integrals. The area integrals are evaluated and stored in universal matrices using techniques similar to those of Silvester [8].

For the portion of the boundary between two adjacent

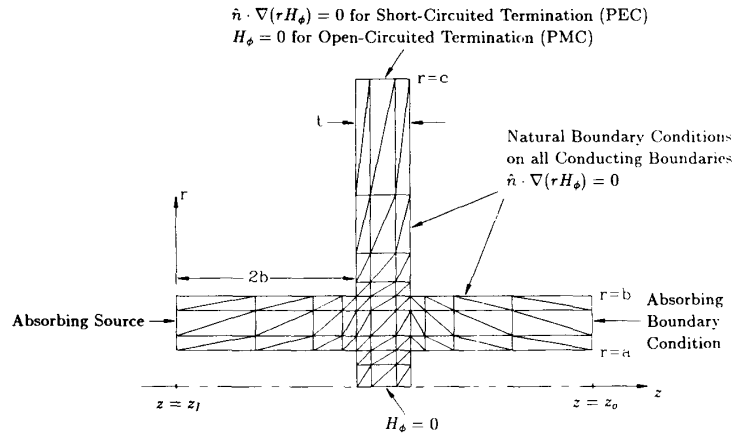


Fig. 4. Finite element mesh with the boundary conditions indicated.

elements, the boundary integrals will sum to zero when  $\hat{n} \cdot \nabla(rH_\phi)/\bar{\epsilon}_r$  is continuous across the boundary. When the total residual equations are assembled, these integrals are replaced by their desired value, zero. This will tend to force  $\hat{n} \cdot \nabla(rH_\phi)/\bar{\epsilon}_r$  to be continuous across the boundary between the elements, which is equivalent to the tangential component of  $\vec{E}$  being continuous across the boundary. The boundary integral also gives the correct "natural boundary condition" for a perfect electric conductor,  $\hat{n} \cdot \nabla(rH_\phi) = 0$ . The boundary conditions for the tangential component of  $\vec{H}(H_\phi)$  and the normal component of  $\vec{E}$  are met by forcing  $H_\phi$  to be continuous across the boundary. The boundary condition for a perfect magnetic conductor and for boundaries with  $r = 0$  is  $H_\phi = 0$ .

At the input port a boundary condition that will inject the incident wave and absorb the reflected wave is needed, and at the output port a boundary condition that will absorb the transmitted wave is needed. These boundary conditions are derived assuming that only the TEM mode exists at the input and output ports. The boundary conditions are derived from the differentiated transmission line equations; for the input port,

$$\left. \frac{dH_\phi}{dz} \right|_{z=z_i} = -jk(2H_i - H_\phi) \quad (16)$$

where  $H_i$  is the value of the incident field at the input port, and for the output port,

$$\left. \frac{dH_\phi}{dz} \right|_{z=z_o} = -jkH_\phi. \quad (17)$$

These boundary conditions are applied by substituting them into the boundary integrals; then, the boundary integrals are evaluated and stored in universal matrices in a manner similar to that used for the area integrals.

The reflection coefficient  $\rho$  and transmission coefficient  $\tau$  are obtained from the fields at the input and output ports. The fields at the input and output ports are essentially TEM; thus,  $rH_\phi$  should be constant at the ports; however,  $rH_\phi$  calculated with the FEM will not be exactly constant due to numerical errors. To minimize the effects of these

numerical errors,  $\rho$  and  $\tau$  are calculated from the average values of  $rH_\phi$  over the cross section of the coaxial line at the input and output ports. The reflection coefficient is the ratio of the reflected wave to the incident wave:

$$\rho = \frac{1}{n_i} \sum_{z=z_i} \frac{rH_\phi - rH_i}{rH_i} = \frac{1}{n_i} \sum_{z=z_i} \frac{H_\phi - H_i}{H_i} \quad (18)$$

where  $n_i$  is the number of nodes on the input port. The transmission coefficient is the ratio of the transmitted wave to the incident wave:

$$\tau = \frac{1}{n_o} \sum_{z=z_o} \frac{H_\phi}{H_i} \quad (19)$$

where  $n_o$  is the number of nodes on the output port.

#### IV. RESULTS

The dielectric properties of two materials with known permittivity were measured to experimentally verify the technique. Fig. 5 is a sketch of the fixture that was constructed for the experiment. Plastic alignment plates with steel alignment pins are used to keep the fixture aligned. Each of the center conductors is supported by the bead in the connector. The diameter of the outer conductor of the coaxial lines is  $2b = 7$  mm and that of the inner conductor is  $2a = 3.04$  mm, and  $c/b = 10$ . Fourth-order elements are used in the finite element mesh, and the number of elements and nodes in the mesh varies from 74 elements with 681 nodes to 178 elements with 1529 nodes depending on the thickness of the sample.

Five different samples of Teflon were measured. The thicknesses of the samples vary from  $t/b = 0.113$  to 1.38, and the samples are approximately 9 cm square. The transmission coefficient of the fixture was measured with a Hewlett Packard 8510 network analyzer in the stepped CW mode with a synthesized source of each of the samples. The magnitude and phase of the measured transmis-

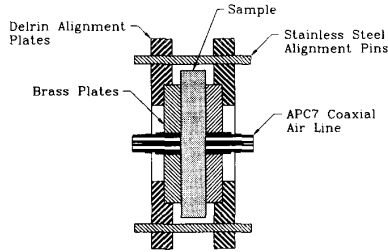


Fig. 5. Cross section of the measurement fixture used in the experiments.

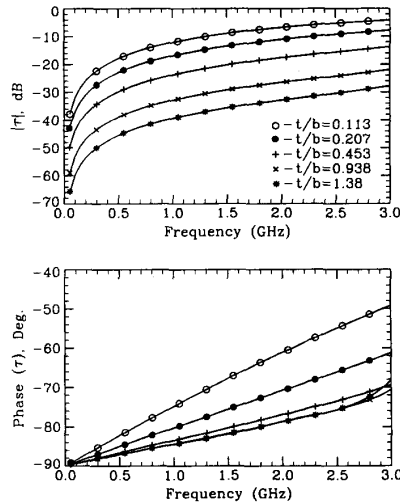


Fig. 6. Magnitude and phase of the measured transmission coefficients as a function of frequency for the five Teflon samples.

sion coefficients are graphed in Fig. 6 as a function of frequency. The magnitude is seen to vary from approximately  $-70$  dB to  $-4$  dB, and the phase is seen to vary approximately linearly with the frequency. The magnitude is smallest for the lowest frequencies and the thickest samples. The lower frequency limit for the technique is determined by the smallest transmission coefficient that can be accurately measured (both magnitude and phase). These measured transmission coefficients were inverted with a numerical root-finding routine using the finite element model for the fixture to obtain the complex relative permittivity of the samples.<sup>1</sup> The real and imaginary parts of the complex permittivity  $\tilde{\epsilon}_r = \tilde{\epsilon}' - j\tilde{\epsilon}''$  are graphed as a function of frequency for the five samples in Fig. 7. Note the expanded vertical scales on the graphs. The values of  $\tilde{\epsilon}'$  are seen to vary from approximately 2.02 to 2.15. The samples were obtained from a local supplier and were not cut from the same block of material; thus, the differences in the measured permittivities in Fig. 7 may be due to actual differences in the samples. Other investigators have obtained values from 2.01 [9] to 2.1 [10]. Most of the values of  $\tilde{\epsilon}''$  are seen to be between

<sup>1</sup>The inversion program was run on a mainframe computer; however, it could be easily run on a personal computer.

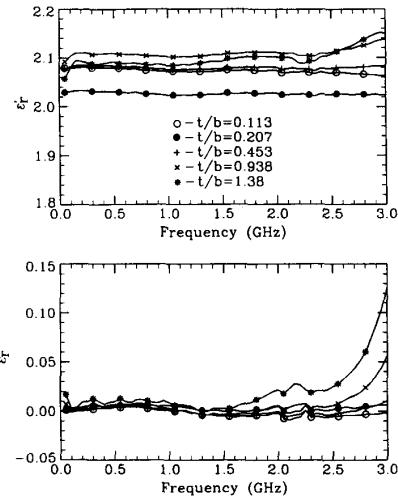


Fig. 7. Real and imaginary parts of the measured complex permittivities as a function of frequency for the five Teflon samples.

$-0.01$  and  $0.01$ . The actual value of  $\tilde{\epsilon}''$  is much smaller than  $0.01$ . The reason for the inaccuracies in the measured values of  $\tilde{\epsilon}''$  is that a small error in the measured transmission coefficient can result in a large error in  $\tilde{\epsilon}''$  for a low-loss material. For the two thickest samples, the apparent  $\tilde{\epsilon}''$  is seen to increase rapidly above  $2.5$  GHz; this is due to part of the energy being radiated out of the open end of the radial transmission line. Since the open end is modeled as a perfect open, the radiated energy is not taken into account in the model; thus, the radiated energy is interpreted as loss in the material. The thickest sample is approximately  $1/7$  of a wavelength thick at  $3$  GHz. The perfect open-circuited termination is not a very good model for the open end when the spacing of the radial line is this thick.

Two different samples of alumina (Wesco AL-995) were measured. The thicknesses of the samples are  $t/b = 0.219$  and  $0.441$ , and the samples are  $7$  cm in diameter. The magnitude and phase of the measured transmission coefficients are graphed in Fig. 8 as a function of frequency for the two samples. The magnitude is seen to vary from approximately  $-40$  dB to  $-5$  dB, and the phase is seen to vary approximately linearly with frequency. These measured transmission coefficients were inverted, and the real and imaginary parts of the complex permittivity obtained. These are graphed as a function of frequency for the two samples in Fig. 9. The values of  $\tilde{\epsilon}'$  are seen to be approximately  $9.25$  for the thicker sample and  $9.6$  for the thinner sample. The value of  $\tilde{\epsilon}''$  is seen to be approximately  $0.05$ . The manufacturer's data sheet for the alumina indicates that  $\tilde{\epsilon}' = 9.58$  and  $\tilde{\epsilon}'' = 0.003$  at  $10$  MHz; and  $\tilde{\epsilon}' = 9.30$  and  $\tilde{\epsilon}'' = 0.01$  at  $1$  GHz. The differences in the measured permittivity for the two different thickness samples are not due to actual differences in the permittivity of the samples but are most likely due to a variation in the contact capacitance between the ends of the center conductors and the samples.

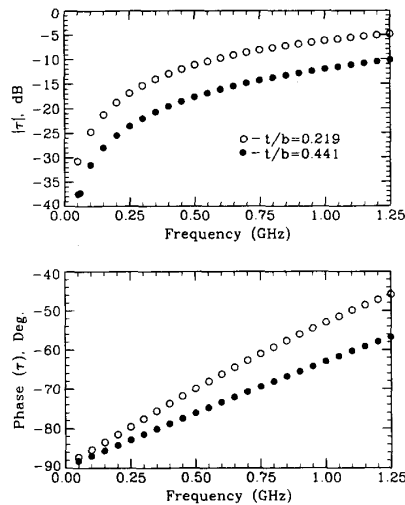


Fig. 8. Magnitude and phase of the measured transmission coefficients as a function of frequency for the two alumina samples.

To explain how the contact capacitance can affect the measured permittivity, consider the simple model sketched in Fig. 10 where the sample is placed in an ideal parallel-plate capacitor. This is an approximate model for the capacitance between the center conductors. In the mode, a thin air gap exists between the sample and the plates of the capacitor. In the ideal case, the gap has zero thickness and the capacitance is

$$C_{\text{Ideal}} = \frac{A\tilde{\epsilon}_s}{t} \quad (20)$$

where  $A$  is the cross-sectional area of the capacitor and  $t$  is the thickness of the sample. In an actual measurement, the gap may have a finite thickness; then

$$C_m = \frac{A\tilde{\epsilon}_s\epsilon_o}{2g\tilde{\epsilon}_s + t\epsilon_o} \quad (21)$$

where  $g$  is the thickness of the gaps. If the capacitance  $C_m$  is measured and the capacitor is treated as if there was no gap, the permittivity obtained,  $\tilde{\epsilon}_m = C_m t/A$ , would be in error. The percentage error in the permittivity is

$$E_\epsilon = 100 \left| \frac{\tilde{\epsilon}_s - \tilde{\epsilon}_m}{\tilde{\epsilon}_s} \right| = 100 \left| \frac{C_{\text{Ideal}} - C_m}{C_{\text{Ideal}}} \right| \\ = \frac{100}{|1 + t\epsilon_o/2g\tilde{\epsilon}_s|} \quad (22)$$

The error is zero when  $g = 0$ . The error is 4% when  $t/g = 500$  and  $\tilde{\epsilon}_s/\epsilon_o = 10$ . The thickest sample of alumina was 1.543 mm thick. Thus, an air gap of only  $g = 1.543/500 \approx 0.003$  mm ( $\approx 0.0001$  inch) would cause a 4% error in the measured permittivity for the sample. Note that for a small error, the error is approximately proportional to the permittivity of the sample; thus, the gap is more of a problem for higher permittivity samples.

To try to minimize the effect of the contact capacitance,

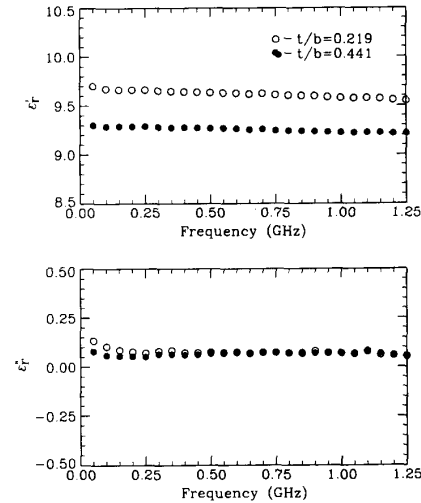


Fig. 9. Real and imaginary parts of the measured complex permittivities as a function of frequency for the two alumina samples.

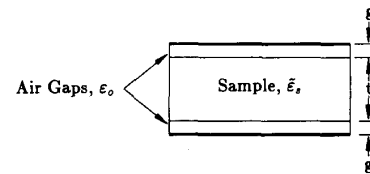


Fig. 10. Model for the contact capacitance of the center conductors, assuming an ideal parallel plate capacitor model.

two techniques were tried. In the first technique, small drops of water were placed on the ends of the center conductors before the sample was placed in the fixture. The water then fills the gap when the fixture is assembled. Since the water has a relatively high permittivity, approximately 80, the error should be reduced by approximately a factor of 80. In the second technique, small drops of silver paint were placed on the ends of the center conductors before the fixture was assembled. The paint is allowed to dry after the fixture is assembled. The paint would then fill the gaps. This should eliminate the contact capacitance. The problem with both of these techniques is that it is hard to get the correct amount of water or paint into the gap. If too little is used, the gap is not filled; and if too much is used, the water or paint is forced out of the gap and will introduce another error. Neither one of these techniques is completely satisfactory. The measurements for the alumina were made using the water drops. The inaccuracy in choosing the amount of water is the reason for the differences in the values of the permittivities for the two samples. The measurements for the Teflon were made without using the water or paint drops. It is not known whether the differences in the measured permittivities between the Teflon samples are due to actual differences, contact capacitances, or other errors.

Another way of dealing with the contact capacitance is

to metalize the portions of the sample that contact the fixture. This technique works well, but it requires that the sample be accurately metalized and placed in the fixture so that it is accurately aligned with the center conductors.

The best solution is to build a fixture that is mechanically rigid. The center conductors for the fixture used in this work are supported by only the connector beads and, thus, cannot be pressed up against the sample with much force. If the mechanical support for the center conductors were much stronger, the center conductors could be pressed against the sample with greater force which would help eliminate the gap.<sup>2</sup> In addition, the faces of the fixture could be machined more accurately by lapping them after the center conductor is installed. This would help eliminate the gap, since the end of the center conductor would be flatter and more closely parallel to the conducting plate.

### V. CONCLUSIONS

A technique for measuring the constitutive parameters of materials over a broad range of frequencies was developed in this work. The technique was experimentally verified by measuring the permittivity of Teflon and alumina samples. Even though both the Teflon and the alumina used in the verification are low-loss materials, the technique is valid for materials with moderate and high loss. The lower frequency limit of the technique is primarily set by the capacitance between the center conductors. At

<sup>2</sup>The mechanical support for the center conductor could be made stronger by pressing a hard plastic bead into the air lines or by using semirigid coaxial lines instead of the air lines.

lower frequencies, the transmission coefficient becomes very small, because the capacitive coupling between the center conductors is very small; the inaccuracies in measuring the small transmission coefficient set the lower frequency limit. The upper frequency limit is set primarily by the thickness of the sample and the outer diameter of the radial line. The sample must be sufficiently thin so that the open end of the radial line does not radiate a significant amount, and the outer radius of the radial line sets the range for which the ratio  $|Y_r/Y_c|$  is large.

### REFERENCES

- [1] M. A. Saed, "A method of moments solution of a cylindrical cavity placed between two coaxial transmission lines," *IEEE Trans. Microwave Theory Tech.*, vol. 39, pp. 1712-1717, Oct. 1991.
- [2] M. R. Taherian, D. J. Yuen, T. M. Habashy, and J. A. Kong, "A coaxial-circular waveguide for dielectric measurement," *IEEE Trans. Geosci. Remote Sensing*, vol. 29, Mar. 1991.
- [3] N. E. Belhadj-Tahar, A. Fourier-Lamer, and H. Chanterac, "Broadband simultaneous measurement of the complex permittivity and permeability using a coaxial line," *IEEE Trans. Microwave Theory Tech.*, vol. 38, pp. 1-7, Jan. 1990.
- [4] S. Ramo, J. R. Whinnery, and T. V. Duzer, *Fields and Waves in Communication Electronics*, 2nd ed. New York: John Wiley & Sons, 1984, ch. 9.
- [5] D. S. Burnett, *Finite Element Analysis from Concepts to Applications*. Reading, MA: Addison-Wesley, 1987.
- [6] W. R. Scott, Jr., "Accurate modeling of axisymmetric two-port junctions in coaxial lines using the finite element method," *IEEE Trans. Microwave Theory Tech.*, vol. 40, pp. 1712-1716, Aug. 1992.
- [7] P. P. Silvester and R. L. Ferrari, *Finite Elements for Electrical Engineers*, 2nd ed. Cambridge, England: Cambridge University Press, 1990.
- [8] P. Silvester, "Construction of triangular finite element universal matrices," *Int. J. Numer. Meth. Eng.*, vol. 12, pp. 237-244, 1978.
- [9] D. W. Gray, *American Institute of Physics Handbook*. New York: McGraw Hill, 1972.
- [10] R. K. Hoffmann, *Handbook of Microwave Integrated Circuits*. Norwood, MA: Artech House, 1987.